International Journal of Mechanical Sciences 259 (2023) 108621

Contents lists available at ScienceDirect

International Journal of Mechanical Sciences

journal homepage: www.elsevier.com/locate/ijmecsci

# Quantitative analysis of acoustic black hole property by the catastrophe theory

Jia Min Niu [a], Jiu Hui Wu [a,b,*], Xiao Li Liu [a], Meng Qi Yuan [a], Li Bo Wang [a]

[a] School of Mechanical Engineering, Xi'an Jiaotong University, Xi'an 710049, China
[b] State Key Laboratory for Strength and Vibration of Mechanical Structures, Xi'an Jiao tong University, Xi'an 710049, China

ARTICLE INFO

*Keywords:*
Acoustic black holes
Catastrophe theory
Quantitative analysis
Hyperbolic umbilical model
Energy focusing

ABSTRACT

Acoustic black holes (ABHs) have garnered increasing attention in the field of vibration and noise reduction due to their excellent wave aggregation effect. A large number of studies have been conducted in analyzing ABH structures, these analytical methods such as finite element and semi-analytical modeling, however, still suffer from limitations in the quantitative analysis of ABHs. The majority of the existing methodologies are intricate and computationally burdensome and do not furnish a quantitative assessment of the ABH structure. To meet this need, we design a theoretical analysis model from the catastrophe theory perspective. Based on the Hyperbolic umbilic model, the proposed analytical method can investigate the quantitative relationships among each parameter and their energy aggregation effects in ABHs. Combined with a dimensionless analytical solution, the underlying mechanism and the quantitative property of ABHs are expected to be revealed with significantly reduced computational complexity. Further, the proposed quantitative method is demonstrated by a numerical simulation test and a practical experiment. The findings illustrate a clear presence of a catastrophe effect across the range of ABH parameter variation, and establish a direct correlation between each ABH parameter and the ABH effect in the proposed approach. The proposed theoretical method holds significant potential in analyzing and applying of ABHs.

## 1. Introduction

The ABH structures, which were first proposed by Mironov et al. [1,2], are obtained by a power-law variation in the thickness of the structure [3]. This structure progressively decelerates both the group and phase velocity of the bending wave, thus causing compression of the wave inside the structure along a specific curve [4,5]. Ideally, the wave speed of the bending wave also approaches zero at the tip while the energy is also gathered at the tip [6]. Due to processing technology limitations, the tip of the ABH must have truncation, which causes significant reflection [7]. The addition of a small amount of damping material at the tip of the ABH was found to be effective in dissipating the vibration energy by Krylov et al. [8,9]. O'Boy et al. [10] and Bowyer et al. [11,12] later conducted experimental investigations into the vibration-damping properties of two-dimensional (2D) ABHs.

The aforementioned methods represent the early stages of ABH research. In recent years, ABH research has experienced a new surge in interest. But ABHs' accurate modeling and theoretical analysis are challenging due to the dramatic changes in the wave number of propagating bending waves.

Finite element software modeling is the most commonly used method for ABH analysis, as it is flexible and suitable for analyzing structures with complex geometries. Such as circular indentations [13], grooves on plates [14], double-leaf [15,16], Archimedes spiral shape [17,18], and ring-shaped ABHs [19] have also surfaced. In addition to structural shear, other methods can achieve the equivalent effect of ABH, including placing circular thin plates at regular intervals inside the pipe [20], controlling the structure's mechanical impedance distribution using memory alloy material [21], embedding a gradient arrangement [22], or creating a gradient distribution of the material's Young's modulus [23]. These technologies enable the creation of structures with low wave reflection, ensuring the realization of favorable ABH states. Periodic studies have been conducted in addition to individual cell analyses [24,25], and they all show positive outcomes [26–28]. All these new structures can be analyzed using the finite element method, which can be a valuable simulation and optimization tool for complex systems. However, the computational burden increases significantly as the system undergoes changes, and the method cannot yield the precise

* Corresponding author at: School of Mechanical Engineering, Xi'an Jiaotong University, Xi'an 710049, China.
*E-mail address:* ejhwu@xjtu.edu.cn (J.H. Wu).

https://doi.org/10.1016/j.ijmecsci.2023.108621
Received 18 April 2023; Received in revised form 24 June 2023; Accepted 11 July 2023
Available online 13 July 2023

relationship between the structure's parameters and the system.

In addition to this many modeling approaches are still proposed. Krylov et al. [29] proposed an analytical method based on geometric acoustics. However, the calculation accuracy may not be sufficient for certain applications. Georgiev et al. [30], on the other hand, used the structural impedance to calculate the reflection matrix in ABH. Huang et al. [31] using the Taylor expansion method, and proposed a new method to determine the reflection coefficient [32]. Impedance matrix method [30,33] Transfer matrix method [34,35] can also be well applied to ABH. The Rayleigh-Ritz method is also widely used recently [34,36]. O'Boy et al. [14] used trigonometric functions for modeling rectangular plates. Then researchers have optimized the model by optimizing the basic functions. They examined the Mexican Hat Wavelet function [37] Morlet [38], Daubechies wavelets [39] and Gaussian basis functions [40–43] to obtain results for ABH beams and plates.

Although all of the above methods provide a good analysis of ABH structures, as a result of the nonlinearity involved in ABH vibrations, attaining accurate solutions becomes exceedingly difficult. Previous nonlinear analytical models, such as finite element and semi-analytic modeling, involve complicated solution processes with high computational costs. Furthermore, the exact relationship between each geometric parameter of an ABH and its energy aggregation effect remains elusive.

Given the nonlinear nature of the ABH structure, our primary focus lies on the system's geometric parameters. Catastrophe theory, a theoretical model that is well-equipped to analyze phase transitions, offers a viable solution to surmounting the complexities posed by this nonlinear scenario.

The non-equilibrium phase transition is the phenomenon of shifting a system from one phase to another [44]. Catastrophe theory explain the process of phase transition [45]. Thom et al. [46] posited that all primary catastrophes could be generalized into seven basic forms, as long as the number of control parameters remained below five. The method has widespread use across many fields and boasts incredible potential in the analysis of complex problems. Anirudh used catastrophe theory to classify singularities in electron dispersion [47], and then used a dovetail model for the transitions between different topological singularities [48]. Damian proposed two new spiking neuron models in neural networks using this theory [49].

In recent years, applications of catastrophe theory in mechanics and machinery have also emerged. Catastrophe theory was used for failure prediction [50,51] and modeling of the chip flow angle [52] the force load curve [53]. In mechanics, Liang employed catastrophe theory to investigate turbulent phase transitions [54] and porous metallic materials [55]. Further research about these studies are discussed by Zhou et. al [56].

As can be seen above, the catastrophe theory is stable and effective in solving nonlinear problems. The focus of the method is on the selection of the potential function. In order to create a more efficient ABH structure, it is essential to understand and analyze the underlying physical processes involved in the system. In this paper, we begin by deducing the existence of a phase transition process in the ABH structure. Next, we based on the catastrophe model and generate a new model dependent on the Hyperbolic umbilical catastrophe model to analyze the ABH structure's phase transition process. After solving the model, the quantitative relationships between each geometric parameter of ABH and the energy aggregation effect can be obtained and the power law value of each relationship can be found. This analysis will enable the establishment of a direct relationship between the geometric parameters and the overall performance of the ABH structure.

The structure of this study is as follows. In Section 2, we explicate the modeling principle of catastrophe theory and elucidate the process of constructing a new catastrophe model, all while introducing the Hyperbolic umbilical catastrophe model. Subsequently, we substitute the vibration problem of ABH into the catastrophe model to obtain the proportional relationship between each ABH parameter and vibrational velocity of the tip of the structure. In Section 3.1, we acquire the ABH model using Comsol and employ finite element simulation results to verify the theory-derived conclusions from Section 2. Section 3.2 confirms the accuracy of the simulations from Section 3.1 with available experimental results. We present our conclusions in Section 4.

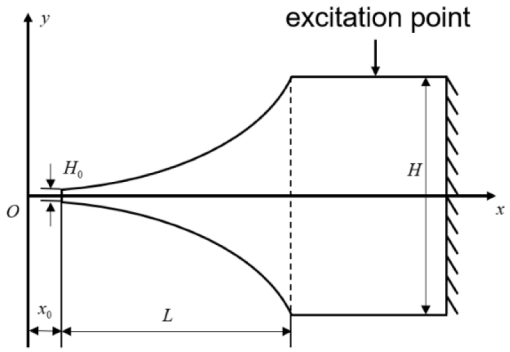


**Fig. 1.** ABH structure with truncation.

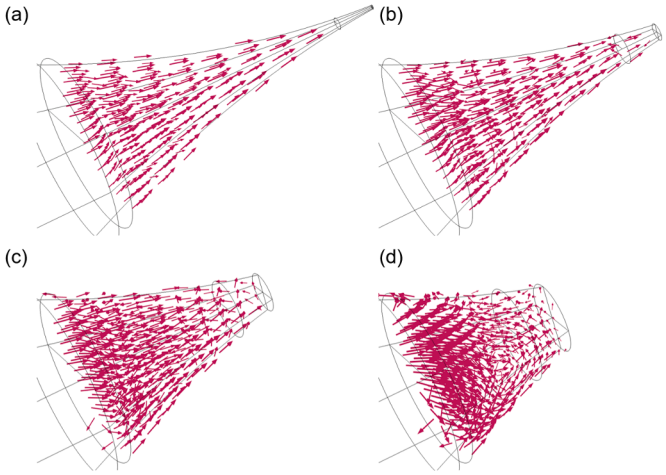


**Fig. 2.** Energy flow diagram of ABHs.

## 2. ABH property analysis based on the catastrophe theory

ABH structures show remarkable aggregation effects on elastic waves, thereby rendering it a promising structure for energy harvesting. In the process of practical engineering applications, however, the abrupt changes in the wave numbers of ABH structures make it hardly possible to obtain exact solutions. Therefore, it is preferable to ignore process intricacies during vibration and then concentrate on deriving quantitative correlations between physical model parameters. In this regard, unknown quantities of ABH structures are expected to derive with known quantities through means of proportional relationships. As previously stated, we have chosen catastrophe theory for our analytical model. Our first step is to assess the suitability of this model in relation to the research object presented in this paper.

### 2.1. Adoption of the catastrophe model

ABH beam is analyzed to demonstrate the derivation process of the proposed ABH model. Fig. 1 illustrates the research object, which is subject to fixed boundary conditions. The curve of ABH is $H = \varepsilon^* x^m$, $H$ denotes the thickness of the homogenous part, $H_0$ to the truncation height of the ABH center, $L$ and $x_0$ to the length and the truncated position of the ABH part, respectively, and ω to the input excitation frequency.

**Table 1**
The seven catastrophe models.

| Catastrophe models | Number of state variables | Number of control variables | Potential function | Equilibrium surface equation |
|---|---|---|---|---|
| Fold | 1 | 1 | $V_F = x^3 + tx$ | $3x^2 + t = 0$ |
| Cusp | 1 | 2 | $V_C = x^4 + tx^2 + ux$ | $4x^3 + 2tx + u = 0$ |
| Swallowtail | 1 | 3 | $V_S = x^5 + ux^3 + vx^2 + wx$ | $5x^4 + 3ux^2 + 2vx + w = 0$ |
| Butterfly | 1 | 4 | $V_B = x^6 + tx^4 + ux^3 + vx^2 + wx$ | $6x^5 + 4tx^3 + 3ux^3 + 2vx + w = 0$ |
| Hyperbolic umbilic | 2 | 3 | $V_H = x^3 + y^3 + txy - ux - wy$ | $\begin{cases} 3x^2 + ty - u = 0 \\ 3y^2 + tx - w = 0 \end{cases}$ |
| Elliptic umbilic | 2 | 3 | $V_E = x^3/3 - xy^2 + w(x^2 + y^2) - ux + vy$ | $\begin{cases} 3x^2 - y^2 + 2wx - u = 0 \\ -2xy + 2wy + v = 0 \end{cases}$ |
| Parabolic umbilic | 2 | 4 | $V_P = y^4 + x^2y + wx^2 + ty^2 - ux - vy$ | $\begin{cases} 2xy + 2wx - u = 0 \\ 4y^3 + x^2 + 2ty - v = 0 \end{cases}$ |

We first conduct a preliminary analysis of the study subjects utilizing Comsol. In Fig. 1, the unit excitation is applied at a designated point. The specific simulation parameters and settings will be comprehensively described in the simulation section of Section 3. When the excitation is set at 3000 Hz, the response corresponding to various $L$values is analyzed using the energy flow method.

Fig. 2 reveals that when $L$ is large, such as in Fig. 2(a), the energy flow demonstrates a parallel and relatively regular flow line. And the energy is also concentrated towards the tip of the beam. At this time, the vibration amplitude of the bending wave is enhanced, and the ABH structure also shows a strong energy aggregation effect. As $L$ decreases, some of the energy flow is reflected (as observed in Fig. 2(b)). However, most of the bending waves still tend to converge towards the tip. As $L$ continues to vary, as shown in Fig. 2(c) and Fig. 2(d), the energy flow line becomes increasingly reflective and disorganized. As $L$ further decreases, the disorder of the flow lines also intensifies. This leads to energy being distributed throughout the beam in various positions, causing the structure to lose the effect of energy aggregation.

By analogy with our most familiar solid-liquid first-order phase transition. When the molecules are arranged in a neat manner, the substance assumes a solid state. As the ambient temperature rises, the molecules begin to lose this arrangement and progressively become more disordered. Eventually, the substance transforms into a liquid state. Analogously, we refer to the state of energy flow with relatively regular streamlines as the phase that demonstrates the ABH effect. The state with disordered energy flow lines refers to the phase without the ABH effect. In these two phases, the same parameters exhibit different power-law relationships with the response of the system. We verify these findings in the subsequent Section 3 utilizing simulations.

That is why the vibration process can be characterized in ABH structure as a transition from one steady state to the other, which is consistent with variation patterns in the catastrophe theory. Thus, the catastrophe theory is introduced in this study.

As we all know, the state function of a system takes unique extreme values when the system is in steady states. Consequently, the change of system state can be transformed into that of change of the extreme values. Mathematically, the system state function can be expressed as $F_{V_1,\ldots,V_m}(x_1, x_2, \ldots, x_n)$, where $V_1,\ldots, V_m$ are influence factors of system, $x_1, x_2, \ldots, x_n$ are state variables. The threshold points for the state change of the system are points that satisfy the potential function equal to 0, that is, solving the following partial differential equation:

$$\frac{\partial}{\partial x_i} F_{V_1,\ldots,V_m}(x_1, x_2, \ldots, x_n) = 0, \quad i = 1, \ldots, n$$

According to the catastrophe theory, there are seven basic types of different properties in Table 1, where $x$, $y$ are state variables, and $t$, $u$, $v$, $w$ are control variables.

To enable a better study of the energy aggregation effect within ABH beam, selecting the appropriate catastrophe model for analyzing the entire system becomes crucial to the analysis.

The behavior of a one-dimensional ABH is influenced by several variables, including ABH length $L$, maximum height $H$, modulus of elasticity $E$, density ρ, tip vibration speed $v$ and frequency ω. Since both $L$ and $H$ have an impact on the structural dimensions of ABH beam, similar to the previous analysis in Fig. 2, we discovered that: when $L$ is fixed, there exists a critical height $H_0$ at the tip, below which the ABH state occurs, leading to the concentration of most of the energy at the tip. Similarly, when $H$ is fixed, there is a critical length $L_0$ that triggers the ABH state.

Thus, by observing the changes in $L$ and $H$, we can reveal the changing state of ABH in our chosen catastrophe model. We designate $L$ and $H$ as state variables. For the problem we are investigating, the chosen model must be capable of revealing the effects of both state variables on the state of the system. We discovered that the Hyperbolic umbilical model places the two state variables in symmetric positions, allowing each change in the two variables to be accurately captured without the small change in one variable being masked by the other. Therefore, we substitute the Hyperbolic umbilical model for the calculation. At this point, the potential function equation is expressed as follows:

$$V = L^3 + H^3 + tLH - uL - wH \tag{1}$$

The equation for the corresponding equilibrium surface is:

$$\begin{cases} 3L^2 + tH - u = 0 \\ 3H^2 + tL - w = 0 \end{cases} \tag{2}$$

We chose the model based on the system under investigation and developed the corresponding system equations. To ensure a more all-encompassing analysis of the ABH state, it is necessary to introduce all variables that impact the system within the model.

### 2.2. Exact derivation of abh property by non-dimensional analysis

We include additional variables that would have an effect on the system as described in the previous section and expand the column of control variables. To obtain the impact of multiple parameters on the system's phase transition properties, we expand the potential function of the two-dimensional collapsed catastrophe model into a multi-dimensional multiple multivariate improved collapsed catastrophe model function. By expressing the control variables $t$, $u$, and $w$ in the model shown in Eq. (3), where A, B, and C are constants and $\alpha_1,\alpha_2,\alpha_3,\alpha_4$ represent the power exponent ofω, ρ, $E$, $v$, we can express $t$, $u$, and $w$ using the following set of equations:

$$\begin{cases} t = A\omega^{\alpha_1}\rho^{\alpha_2}E^{\alpha_3}v^{\alpha_4} \\ u = B\omega^{\alpha_1}\rho^{\alpha_2}E^{\alpha_3}v^{\alpha_4} \\ w = C\omega^{\alpha_1}\rho^{\alpha_2}E^{\alpha_3}v^{\alpha_4} \end{cases} \tag{3}$$

When Eq. (3) is substituted into Eq. (2), a potential function with multiple parameters and dimensions is obtained. Nonetheless, this equation is not closed, and the number of variables exceeds the number of equations. As a result, the quantitative relationship between physical quantities in the system cannot be resolved. To address this issue, we introduce the dimensionless analysis method and establish new equilibrium relations. This allows us to extend the equation and solve for the relationship between variables. We select M (mass), T (time), and L (length) as the fundamental dimensions. This is because every other derived quantity can be expressed either by definition or according to

**Table 2**
Dimensional relationship of the four physical quantities.

| | $\omega$ | $\rho$ | $E$ | $\nu$ |
|---|---|---|---|---|
| L | 0 | −3 | −1 | 1 |
| T | −1 | 0 | −2 | −1 |
| M | 0 | 1 | 1 | 0 |

objective laws as a combination of these three basic dimensions. And we derive the following Table 2 of dimensions for each variable:

It is crucial that any equation that reflects a physical law must have equivalent dimensions of each physical quantity on both the left and right sides. Hence, dimensional analysis also delivers an equilibrium equation for determining the quantitative relationship of a system at a specific state. By employing this principle, we can deduce from Eq. (2) the dimensional units of the control variables to be $t \rightarrow [L^1]$,$u \rightarrow [L^2]$,$w \rightarrow [L^2]$.

We can analyze Eq. (2) by considering the length $L$ corresponding to the ABH part as the object of analysis. To ensure dimensional homogeneity on both sides of the equation for $t$, we obtain the following set of equations:

$$\begin{cases} -3\alpha_2 - \alpha_3 + \alpha_4 = 1 \\ -\alpha_1 - 2\alpha_3 - \alpha_4 = 0 \\ \alpha_2 = -\alpha_3 \end{cases} \tag{4}$$

$$\begin{cases} -3\alpha_2 - \alpha_3 + \alpha_4 = 2 \\ -\alpha_1 - 2\alpha_3 - \alpha_4 = 0 \\ \alpha_2 = -\alpha_3 \end{cases} \tag{5}$$

From, Eq. (3), Eq. (4) and Eq. (5), the control variables $t$ and $u$ can be derived.

$$\begin{cases} t = A\omega^{-1}\rho^{\frac{\alpha_4-1}{2}}E^{\frac{1-\alpha_4}{2}}\nu^{\alpha_4} \\ u = B\omega^{-2}\rho^{\frac{\alpha_4-2}{2}}E^{\frac{2-\alpha_4}{2}}\nu^{\alpha_4} \end{cases} \tag{6}$$

The equation mentioned above is obtained by substituting Eq. (6) into Eq. (2):

$$3L^2 + H{\cdot}A\omega^{-1}\rho^{\frac{\alpha_4-1}{2}}E^{\frac{1-\alpha_4}{2}}\nu^{\alpha_4} - B\omega^{-2}\rho^{\frac{\alpha_4-2}{2}}E^{\frac{2-\alpha_4}{2}}\nu^{\alpha_4} = 0 \tag{7}$$

As A and B are arbitrary constants, we consider their universality and establish $B = 0$ in the aforementioned equation, which represents the most uncomplicated scenario encompassing all variables. Let the cut-on frequency of ABH be $\omega_{cut\_on}$, and because the alteration of $\omega_{cut\_on}$ is irrespective of the value of $\nu$, we set $\alpha_4 = 0$. Upon deriving the equation of the catastrophe point for the frequency$\omega$, we arrive at the cut-on frequency $\omega_{cut\_on}$, the following formula is presented:

$$3L^2 + AH\omega_{cut\_on}^{-1} \times \rho^{-1/2} \times E^{1/2} = 0 \tag{8}$$

The cut-on frequency ABH can be acquired by solving Eq. (8),

$$\omega_{cut\_on} = AL^{-2}HE^{1/2}\rho^{-1/2} \tag{9}$$

The findings we obtained are aligned with those derived from theoretical derivations in the literature [57], demonstrating the accuracy and validity of the research model utilized in our study. Additionally, $\omega_{cut\_on}$ can be used as frequency critical point to differentiate between the two ABH phases.

Subsequently, the catastrophe feature of $L$ can be computed by solving for $\nu$ using Eq. (7):

$$\nu = -3L^{\frac{2}{\alpha_4}}\left(A\omega^{-1}\rho^{\frac{\alpha_4-1}{2}}E^{\frac{1-\alpha_4}{2}}H - B\omega^{-2}\rho^{\frac{\alpha_4-2}{2}}E^{\frac{2-\alpha_4}{2}}\right)^{-\frac{1}{\alpha_4}} \tag{10}$$

Using a similar methodology, we derive the catastrophe property of $H$. Assuming the length L of the ABH is constant, we analyze the vibrational velocity of the tip of the structure $\nu$ that corresponds to the tip height $H_0$. Taking the partial derivative of Eq. (2) gives: $3H^2 + tL - w = 0$. Substituting the extended control variables obtained in the previous section through Eq. (3), we arrive at:

$$\nu = -3H^{\frac{2}{\alpha_4}}\left(A\omega^{-1}\rho^{\frac{\alpha_4-1}{2}}E^{\frac{1-\alpha_4}{2}}L - C\omega^{-2}\rho^{\frac{\alpha_4-2}{2}}E^{\frac{2-\alpha_4}{2}}\right)^{-\frac{1}{\alpha_4}} \tag{11}$$

The equation obtained provides insight into the multidimensional vibrational process between the tip velocity $\nu$ and the remaining variables.

It is essential to note that in Eq. (10) and Eq. (11), this relation is not an exact quantitative relation since it comprises an unknown power exponent $\alpha_4$. Consequently, it can only be deemed a semi-quantitative relation. To analyze this relation, we employed MATLAB.

### 2.3. The quantitative relationship between ABH parameters and ABH effects

By substituting the remaining variables in the system, we can derive a 3D plot using MATLAB to reveal the relationship between the tip velocity $\nu$ and $L$, as depicted below:

In Fig. 3(a) we can obtain the relationship between the length$L$ of the ABH section, the power index $\alpha_4$ and the tip velocity $\nu$. Fig. 3(b) is obtained by intercepting the cross section parallel to the $\nu - \alpha_4$ plane in the 3D diagram. From Fig. 3(b), we can get that $\alpha_4$ possesses two special points on the curve. We know from the theory that the special points correspond to the points at which the state of the system changes, thus, these two points also correspond to the two states of ABH, respectively. As previously shown in Fig. 2, when ABH is taking place, the energy flow tends to converge towards the tip of the structure. Hence, the tip is the area with the highest energy, and the vibration at this location is the strongest. As $L$ decreases, the tendency of energy gathering at the tip gradually wanes, leading to a reduction in vibration at the tip. If we compare this process with Fig. 3, when $\alpha_4 = 1.8$, the tip velocity $\nu$ attains its highest value. Therefore, this point $\alpha_4 = 1.8$ corresponds to the status when the ABH effect emerges in the structure. In Fig. 3.2 (b), we observe

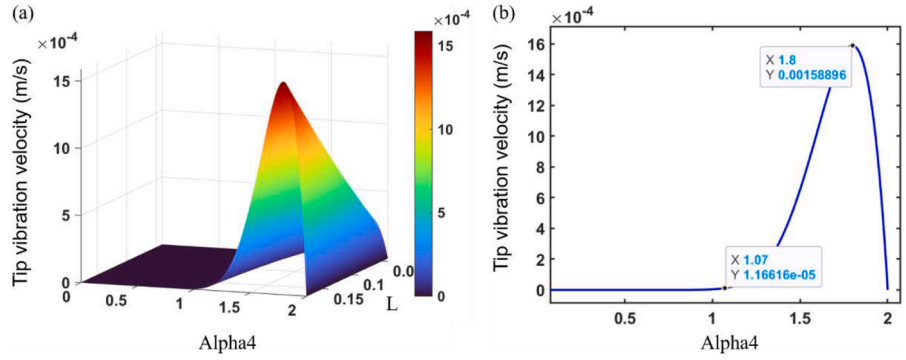


**Fig. 3.** (a) The relationship among ABH length $L$, coefficient $\alpha_4$, and tip velocity $\nu$; (b) The relationship between the tip velocity $\nu$ and coefficient $\alpha_4$.

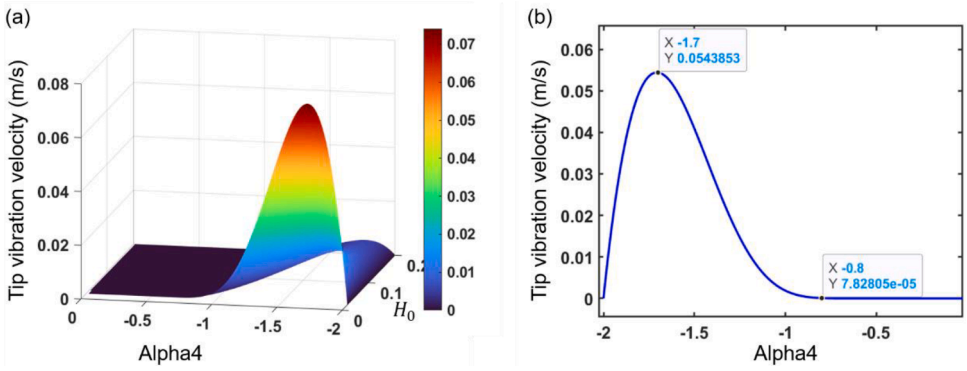


**Fig. 4.** (a) The relationship among ABH tip height $H_0$, coefficient $\alpha_4$, and tip velocity $v$; (b) The relationship between the tip velocity $v$ and coefficient $\alpha_4$.

that$v$ at point $\alpha_4 = 1.07$ is comparatively low, denoting that point $\alpha_4 = 1.07$ corresponds to the state when the ABH effect has not yet taken place.

By substituting $\alpha_4 = 1.07$and $\alpha_4 = 1.8$into Eq. (10), the proportional relationship between the tip velocity $v$ and the ABH length $L$ can be obtained for the two states of the ABH, while keeping the material parameters and geometric parameters of the system constant. As previously mentioned, A and B are arbitrary constants, we consider their universality and establish $B = 0$ in the aforementioned equation, which represents the most uncomplicated scenario encompassing all variables.

From Eq. (10), the quantitative relationship between the tip velocity $v$ and the ABH length $L$ can be expressed as: $v \propto L^{2/\alpha_4}$.

Integrating the aforementioned relationship with Fig. 3(b), it can be inferred that for this particular geometric parameter, the structure exhibits the ABH state when its length ($L$) exceeds the critical threshold, as indicated by the following relationship: $v \propto L^{1.1}$. Conversely, when the length is less than the critical value, the structure does not assume the ABH state, indicated by the following relationship: $v \propto L^{1.87}$.

Using a similar methodology, the velocity relationship with the rest of the variables can be obtained through Eq. (11). To establish a relationship between the tip velocity and $H_0$, the remaining variables in the system are substituted, resulting in a three-dimensional plot in MATLAB as shown in the Fig. 4.

The Fig. 4(a) illustrates the relationship between the ABH tip height $H_0$, power exponent $\alpha_4$, and tip velocity $v$. According to Fig. 4(b) we can obtain, the two special points, $\alpha_4 = -0.8$ and $\alpha_4 = -1.7$, are consistent with our previous analysis and correspond to the two distinct states of the ABH. At point $\alpha_4 = -0.8$, the ABH exhibits low velocity and no ABH state occurs. In contrast, at point $\alpha_4 = -1.7$, the tip velocity increases sharply and the ABH undergoes a catastrophe change in state, with the ABH part in the ABH state and energy concentrated at the tip of the ABH.

From Eq. (10), the quantitative relationship between the tip velocity $v$ and the ABH tip height $H_0$ can be expressed as:.$v \propto H_0^{2/\alpha_4}$

Integrating the aforementioned relationship with Fig. 4(b), it can be inferred that for this particular geometric parameter, the structure exhibits the ABH state when its height ($H$) exceeds the critical threshold, as indicated by the following relationship: $v \propto H_0^{1.17}$. Conversely, when the height is lesser than the critical value, the structure does not assume the ABH state, indicated by the following relationship: $v \propto H_0^{2.5}$.

This section details the establish and analysis of a novel catastrophe analysis method based on the Hyperbolic umbilical model for quantitatively evaluating complex phase transition systems. We apply this model to the object of study in this paper and derive the associated solutions. Our results demonstrate that the ABH beam displays two distinct phases as the geometric parameters vary. Additionally, we establish a power-law relationship between these two phases and the energy absorption effect of the system. In the next section, we further verify our findings through simulation.

**Table 3**
Material parameters and geometric parameters of ABH.

| Geometrical parameters | Material parameters |
|---|---|
| $\varepsilon = 0.005$ | $E = 210$Gpa |
| $m = 2$ | $\rho = 7800$kg/m$^3$ |
| | $\eta = 0.005$ |

where $E$ is the modulus of elasticity, $\rho$ is the material density, and $\eta$ is the material loss factor.

## 3. Simulation and experimental verification

### 3.1. Simulation verification

To validate the accuracy of the proposed ABH model, this section employs finite element simulation results to investigate the vibration of an ABH beam. Specifically, a one-dimensional ABH with a circular cross-section is created, as illustrated in the previous Fig. 1. The uniform part has a diameter of $x$, while the non-uniform part's local radius $H(x)$ is determined by the function $H(x) = \varepsilon * x^m$ relationship. The material and structural parameters are provided in Table 3, where $x_0$ denotes the distance from the edge of the homogeneous part to the coordinate origin, and $x_{ABH}$ represents the demarcation point between the homogeneous and non-homogeneous sections. Due to processing technology constraints, the ABH structure must have a truncated part, which we set at coordinate position $x_0$. In line with the preceding theoretical derivation, two variations of the ABH are depicted in Fig. 5(a) and Fig. 6(a). One involves fixing L and gradually decreasing $H$, while the other entails fixing H and decreasing $L$. To construct the finite element model, the multiphysics field analysis software Comsol Multiphysics is utilized.

In order to improve the analysis of the effect of the ABH section on energy clustering, the fixed uniform length is shortened, and one end is held in place while the other remains free. The excitation is applied at the end of the ABH as a shift with a frequency ranging from 2000 to 5000 Hz, with the direction of loading being perpendicular to the shaft axis of the ABH.

To derive the model, we consider a fixed value of length H for the ABH and varying length $L$. Our simulation object was modeled based on the fundamental unit depicted in Fig. 1. The graph shown in Fig. 5(a) depicts the varying length L of the ABH, with the height H of the ABH being kept constant. The three sections - indicated by arrows in the figure - corresponding toA′, B′, C′, serve as the object of our research. By providing a given displacement input, we can obtain tip velocity for different ABH structural parameters, which can account for the effect of energy clustering. The logarithm of tip velocity versus the ABH length $L$ is plotted in Fig. 5(b) after extracting the tip velocity response.

From Fig. 5, it is clear that the tip velocity increases as $L$ gets larger, which is in line with our observations in Fig. 2 and the analysis in Section 2. However, while the velocity demonstrates an overall upward

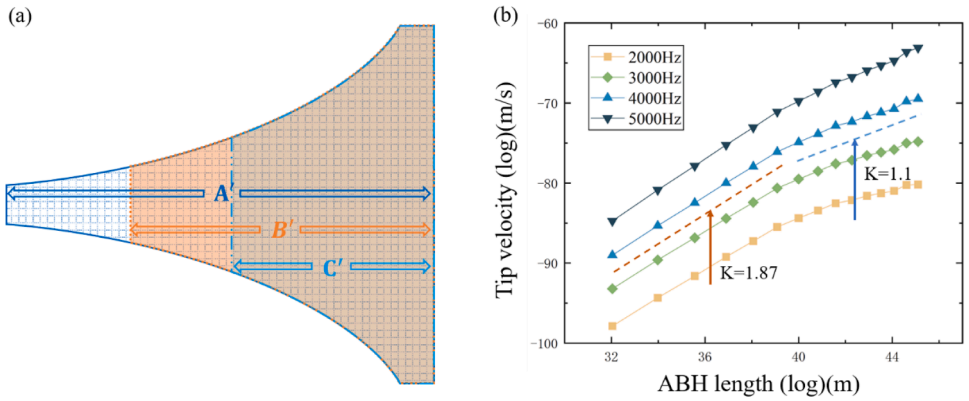


**Fig. 5.** The proportional relationship of variable *L*. (a) *L* is a variable and *H* is a quantitative analysis object; (b) The numerical results of the relationship between the tip velocity and ABH length.

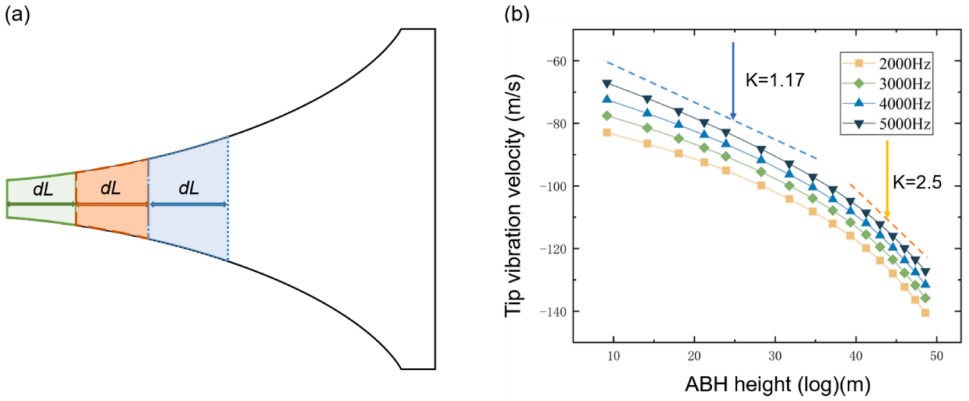


**Fig. 6.** The proportional relationship of variable *H*. (a) *H* is a variable and *L* is a quantitative analysis object; (b) The numerical results of the relationship between the tip velocity and ABH height.

trend, Fig. 5(b) highlights that the velocity growth rate has two distinct stages. When *L* is small, the velocity increase rate is relatively rapid as *L* grows. At this stage, *L* corresponds to Fig. 2(c) and Fig. 2(d), a state where the energy flow does not tend to accumulate at the tip but instead spreads throughout the structure due to a relatively large truncation, resulting in a large number of reflections. Subsequently, as *L* continues to increase, the energy flow starts to move towards the tip, consistent with the comparison of Fig. 2(a) and Fig. 2(b). During this process, the entire structure is in a state with ABH effect.

As the truncation *L* becomes larger, the vibration velocity also increases. Nevertheless, Fig. 5(b) shows that the increase in tip velocity becomes steadily slower as *L* nears a certain point. And after this point, corresponding to Fig. 2(a) and Fig. 2(b), the energy flow gradually begins to enter into an ordered phase. This marks the system is in a stable phase with ABH effects, which we define that point as the critical point. The growth in the left and right velocities near this point exhibits two noticeably different slopes, indicating that the vibrational state of the system is split into two distinct states around this point. Thus, this point represents the state change point, i.e., the phase transition point described in the previous section. This point corresponds with the extreme value point in Fig. 3 of the previous section. The entire process validates our prior deduction that there are indeed two states and catastrophe point of the system as the variables change.

The same approach was used to establish the relationship between the height *H* of the ABH and tip velocity *v*, with $\varepsilon = 0.0016$. We employed the same modeling method to maintain a constant length L but vary the height H of the ABHs, as shown in Fig. 6(a). The region marked by an arrow in the figure corresponds to the object of our research. The resulting response relationship between H and v is shown in Fig. 6(b) when excitation is applied to the end. Analysis of the plots reveals that an increase in H is inversely proportional to tip velocity v, as displayed in Fig. 6(b).When *L* is fixed, the ABH's tip is relatively small, and the velocity of the ABH tip is at its maximum. As *H* increases, *v* gradually decreases at a relatively slow rate. At this point, the structure has the ABH effect and the energy flow lines inside the structure are parallel and directed towards the tip. Subsequently, as the *H* value gradually increases, the catastrophe point appears. Following the catastrophe, the decrease in *v* abruptly increases, and the flow lines within the structure become disordered.

Furthermore, we can calculate the two distinct slopes in Fig. 6(b) and find that they align with the power law relationship derived from our prior theoretical analysis. This represents a validation that our proposed model is effective at quantitatively analyzing the system's phase transition.

In this section, we investigated the phase variation of the entire structure via a combination of simulation and theoretical analysis. As the studied parameters vary, the ABH beam 's entire process divided into two parts via the catastrophe point, leading to the phase with ABH effect and the phase without ABH effect, as proposed in the previous section. Then, we calculated the slopes of these two parts and discovered that the slopes acquired from simulation were in line with those obtained from our theoretical analysis. Therefore, our proposed model can quantitatively analysis the tip velocity and energy aggregation effect of ABH structures of varying sizes, and conclusively derive the associated power-law relationship.

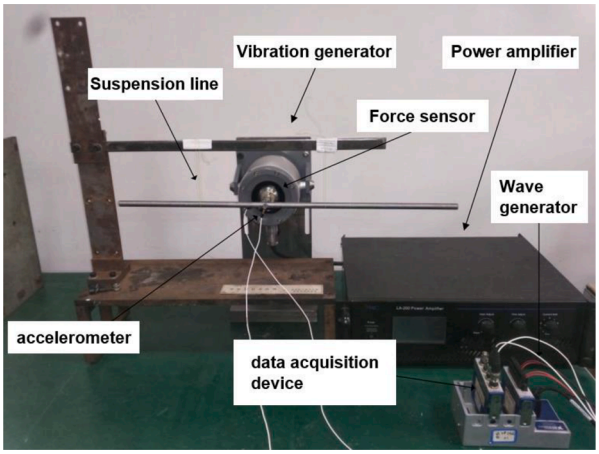


**Fig. 7.** The platform of experiment setting.

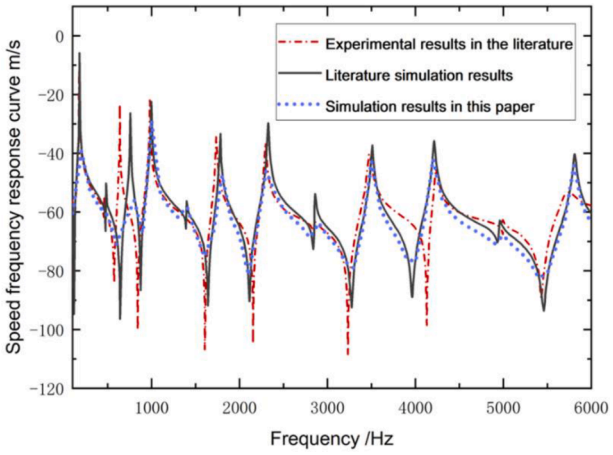


**Fig. 8.** Comparison of experimental results and simulation results.

### 3.2. Experimental verification

As the research subject of this paper is a one-dimensional ABH with a circular cross-section, consistent with the experimental setup detailed in the literature [58], we have utilized these experiments to validate the simulations presented in this study.

Similar to the previous model (Fig. 1), The uniform segment, with a length of 500mm, has been assigned a fixed value of 12mm for the parameter $H$. The non-uniform part $L_{ABH}$ has been set to160mm, and the local radius $H(x)$ at any point in the non-uniform part has been determined based on the relationship $H(x) = A^{*}\varepsilon x^{2}$, where $\varepsilon = 0.00015\text{mm}^{-1}$. The excitation signal utilized is Gaussian white noise with a frequency range of 100 to 6000 Hz, and the system's sampling rate is fixed at 25600 Hz with 25600 sampling points. The experimental facility is shown in Fig. 7:

Simultaneously, we developed an identical simulation model in Comsol, and the outcomes are also depicted in Fig. 6.

From the literature [58], it can be concluded that the experimental results correspond with their simulation results. Additionally, as depicted in Fig. 8, the simulation results of our modeling are also consistent with the corresponding results in [58]. Consequently, the accuracy in modeling settings of our proposed model can be then demonstrated. In addition, the curves in Section 3 generated through modeling can also be verified. These curves in Section 3 reflect a perfect fit with our theoretical derivation, thereby verifying the accuracy of our theory.

## 4. Conclusion

In this study, we present an improved Hyperbolic umbilical catastrophe model for quantitative analyzing the vibration process of ABH. Based on our results and analysis, the following conclusions can be drawn:

(1) We choose the Hyperbolic umbilical catastrophe model as the ABH length $L$ and the tip height $H$ belong to the same magnitude of influence parameters. Additionally, we introduce variable expansion and dimensionless analysis to establish a theoretical analysis model for ABH.
(2) In the context of this study, by substituting ABH-related parameters into the model and solving for catastrophe points using MATLAB, we derive the quantitative relationship between the energy aggregation effect of the ABH and each geometric parameter of the system.
(3) The accuracy of our theoretical analysis is verified through simulations using Comsol. Furthermore, we compare our simulations with existing experiments to demonstrate the correctness of our theoretical derivation.

## CRediT authorship contribution statement

**Jia Min Niu:** Conceptualization, Methodology, Software, Investigation, Formal analysis, Writing – original draft. **Jiu Hui Wu:** Data curation, Writing – original draft. **Xiao Li Liu:** Visualization, Writing – review & editing. **Meng Qi Yuan:** Software, Validation. **Li Bo Wang:** Writing – review & editing.

## Declaration of Competing Interest

The authors declare that they have no known competing financial interests or personal relationships that could have appeared to influence the work reported in this paper.

## Data availability

No data was used for the research described in the article.

## References

[1] Mironov M. Propagation of a flexural wave in a plate whose thickness decreases smoothly to zero in a finite interval. Sov Phys Acoust Ussr 1988;34:318–9.
[2] Mironov MA, Pislyakov VV. One-dimensional acoustic waves in retarding structures with propagation velocity tending to zero. Acoust Phys 2002;48:347–52. https://doi.org/10.1134/1.1478121.
[3] Krylov VV. Geometrical-acoustics approach to the description of localized vibrational modes of an elastic solid wedge. Sov Phys Tech Phys 1990;35:137–40.
[4] Krylov VV, Shuvalov AL. Propagation of localised flexural vibrations along plate edges described by a power law. Inst Acoust 2000;22:263–70.
[5] Conlon S, Fahnline J, Semperlotti F. Numerical analysis of the vibroacoustic properties of plates with embedded grids of acoustic black holes. J Acoust Soc Am 2015;137:447–57. https://doi.org/10.1121/1.4904501.
[6] Krylov VV, Tilman FJBS. Acoustic 'black holes' for flexural waves as effective vibration dampers. J Sound Vib 2004;274:605–19. https://doi.org/10.1016/j.jsv.2003.05.010.
[7] Krylov V. New type of vibration dampers utilising the effect of acoustic "black holes. Acta Acust United Acust 2004;90:830–7.
[8] Kralovic Victor V. Damping of flexural vibrations in tapered rods of power-law profile: experimental studies. © Inst Acoust 2007.
[9] Kralovic V, Bowyer EP, Krylov VV, O'Boy DJ. Experimental study on damping of flexural waves in rectangular plates by means of one-dimensional acoustic "Black Holes. Int. Acoust. Conf. 2009.
[10] Bowyer E, Krylov V. Experimental study of sound radiation by plates containing circular indentations of power-law profile. Appl Acoust 2015;88:30–7. https://doi.org/10.1016/j.apacoust.2014.07.014.
[11] Bowyer E, O'Boy D, Krylov V, Gautier F. Experimental investigation of damping flexural vibrations in plates containing tapered indentations of power-law profile. Appl Acoust 2013;74:553–60. https://doi.org/10.1016/j.apacoust.2012.10.004.
[12] Bowyer EP, Krylov VV. Experimental investigation of damping flexural vibrations in glass fibre composite plates containing one- and two-dimensional acoustic black

holes. Compos Struct 2014;107:406–15. https://doi.org/10.1016/j.compstruct.2013.08.011.
[13] Deng J, Zheng L, Guasch O, Wu H, Zeng P, Zuo Y. Gaussian expansion for the vibration analysis of plates with multiple acoustic black holes indentations. Mech Syst Signal Process 2019;131:317–34. https://doi.org/10.1016/j.ymssp.2019.05.024.
[14] O'Boy DJ, Krylov VV. Vibration of a rectangular plate with a central power-law profiled groove by the Rayleigh–Ritz method. Appl Acoust 2016;104:24–32. https://doi.org/10.1016/j.apacoust.2015.10.018.
[15] Ji H, Liang Y, Qiu J, Cheng L, Wu Y. Enhancement of vibration based energy harvesting using compound acoustic black holes. Mech Syst Signal Process 2019;132:441–56. https://doi.org/10.1016/j.ymssp.2019.06.034.
[16] Ma L, Zhou T, Cheng L. Acoustic Black hole effects in Thin-walled structures: realization and mechanisms. J Sound Vib 2022;525:116785. https://doi.org/10.1016/j.jsv.2022.116785.
[17] Park S, Lee JY, Jeon W. Vibration damping of plates using waveguide absorbers based on spiral acoustic black holes. J Sound Vib 2022;521:116685. https://doi.org/10.1016/j.jsv.2021.116685.
[18] Park S, Kim M, Jeon W. Experimental validation of vibration damping using an Archimedean spiral acoustic black hole. J Sound Vib 2019;459:114838. https://doi.org/10.1016/j.jsv.2019.07.004.
[19] Deng J, Guasch O, Zheng L. Ring-shaped acoustic black holes for broadband vibration isolation in plates. J Sound Vib 2019;458:109–22. https://doi.org/10.1016/j.jsv.2019.06.017.
[20] El-Ouahabi AA, Krylov VV, O'Boy DJ. Investigation of the acoustic black hole termination for sound waves propagating in cylindrical waveguides. In: Int. Conf. InterNoise; 2015. p. 2015.
[21] Georgiev VB, Cuenca J, Bermúdez MMA, Gautier F, Simon L. Recent progress in vibration reduction using Acoustic Black Hole effect. In: ; 2010.
[22] Gao W, Qin Z, Chu F. Broadband vibration suppression of rainbow metamaterials with acoustic black hole. Int J Mech Sci 2022;228:107485. https://doi.org/10.1016/j.ijmecsci.2022.107485.
[23] Huang W, Zhang H, Inman DJ, Qiu J, Cesnik CES, Ji H. Low reflection effect by 3D printed functionally graded acoustic black holes. J Sound Vib 2019;450:96–108. https://doi.org/10.1016/j.jsv.2019.02.043.
[24] Zhao L, Conlon SC, Semperlotti F. Broadband energy harvesting using acoustic black hole structural tailoring. Smart Mater Struct 2014;23:065021. https://doi.org/10.1088/0964-1726/23/6/065021.[3].
[25] Zhao L, Conlon SC, Semperlotti F. An experimental study of vibration based energy harvesting in dynamically tailored structures with embedded acoustic black holes. Smart Mater Struct 2015;24:065039. https://doi.org/10.1088/0964-1726/24/6/065039.
[26] Tang L, Cheng L. Broadband locally resonant band gaps in periodic beam structures with embedded acoustic black holes. J Appl Phys 2017;121:605.
[27] Deng J, Guasch O, Maxit L, Gao N. A metamaterial consisting of an acoustic black hole plate with local resonators for broadband vibration reduction. J Sound Vib 2022;526:116803. https://doi.org/10.1016/j.jsv.2022.116803.
[28] Deng J, Gao N, Chen X, Han B, Ji H. Evanescent waves in a metabeam attached with lossy acoustic black hole pillars. Mech Syst Signal Process 2023;191:110182. https://doi.org/10.1016/j.ymssp.2023.110182.
[29] Krylov VV. Transmission of Rayleigh waves through smooth large-scale surface irregularities. Sov Phys Acoust 1988;34:613–8.
[30] Georgiev VB, Cuenca J, Gautier F, Simon L, Krylov VV. Damping of structural vibrations in beams and elliptical plates using the acoustic black hole effect. J Sound Vib 2011;330:2497–508. https://doi.org/10.1016/j.jsv.2010.12.001.
[31] Huang W, Ji H, Qiu J, Cheng L. Analysis of ray trajectories of flexural waves propagating over generalized acoustic black hole indentations. J Sound Vib 2018;417:216–26. https://doi.org/10.1016/j.jsv.2017.12.012.
[32] Ji H, Luo J, Qiu J, Cheng L. Investigations on flexural wave propagation and attenuation in a modified one-dimensional acoustic black hole using a laser excitation technique. Mech Syst Signal Process 2018;104:19–35. https://doi.org/10.1016/j.ymssp.2017.10.036.
[33] Raybaud G, Lee JY, Jeon W, Pelat A, Gautier F. On the control of the absorption of an Acoustic Black Hole by using attached point supports. J Sound Vib 2023;548:117562. https://doi.org/10.1016/j.jsv.2023.117562.
[34] Guasch O, Arnela M, Sánchez-Martín P. Transfer matrices to characterize linear and quadratic acoustic black holes in duct terminations. J Sound Vib 2017;395:65–79. https://doi.org/10.1016/j.jsv.2017.02.007.
[35] Guasch O, Sánchez-Martín P, Ghilardi D. Application of the transfer matrix approximation for wave propagation in a metafluid representing an acoustic black hole duct termination. Appl Math Model 2020;77:1881–93. https://doi.org/10.1016/j.apm.2019.09.039.
[36] Denis V, Gautier F, Pelat A, Poittevin J. Measurement and modelling of the reflection coefficient of an Acoustic Black Hole termination. J Sound Vib 2015;349:67–79. https://doi.org/10.1016/j.jsv.2015.03.043.
[37] Tang L. Acoustic black hole effect for vibration control 2017.
[38] Zeng P, Zheng L, Deng J, Elsabbagh A, Xiang S, Yan T, et al. Flexural wave concentration in tapered cylindrical beams and wedge-like rectangular beams with power-law thickness. J Sound Vib 2019;452:82–96. https://doi.org/10.1016/j.jsv.2019.04.002.
[39] Li M, Su Z, Li C. A 2D Daubechies wavelet model on the vibration of rectangular plates containing strip indentations with a parabolic thickness profile. J Sound Vib 2018;429:130–46.
[40] Deng J, Guasch O, Zheng L. A semi-analytical method for characterizing vibrations in circular beams with embedded acoustic black holes. J Sound Vib 2020;476:115307. https://doi.org/10.1016/j.jsv.2020.115307.
[41] Deng J, Guasch O, Zheng L. Reconstructed Gaussian basis to characterize flexural wave collimation in plates with periodic arrays of annular acoustic black holes. Int J Mech Sci 2021;194:106179. https://doi.org/10.1016/j.ijmecsci.2020.106179.
[42] Deng J, Gao N. Broadband vibroacoustic reduction for a circular beam coupled with a curved acoustic black hole via nullspace method. Int J Mech Sci 2022;233:107641. https://doi.org/10.1016/j.ijmecsci.2022.107641.
[43] Chen X, Zhao J, Deng J, Jing Y, Pu H, Luo J. Low-frequency enhancement of acoustic black holes via negative stiffness supporting. Int J Mech Sci 2023;241:107921. https://doi.org/10.1016/j.ijmecsci.2022.107921.
[44] Gao J, Guo W, Vinen W. Determination of the effective kinematic viscosity for the decay of quasiclassical turbulence in superfluid He-4. Phys Rev B 2016;94. https://doi.org/10.1103/PhysRevB.94.094502.
[45] Chilver H. Wider implications of catastrophe theory. Nature 1975;254. https://doi.org/10.1038/254381a0. 381–381.
[46] Levyleblond J. Modeles mathematiques morphogenese - Thom,R. Critique 1977;33:430–41.
[47] Chandrasekaran A, Shtyk A, Betouras JJ, Chamon C. Catastrophe theory classification of Fermi surface topological transitions in two dimensions. Phys Rev Res 2020;2:013355. https://doi.org/10.1103/PhysRevResearch.2.013355.
[48] Hu J, Zhang R-Y, Wang Y, Ouyang X, Zhu Y, Jia H, et al. Non-Hermitian swallowtail catastrophe revealing transitions among diverse topological singularities. Nat Phys 2023:1–6. https://doi.org/10.1038/s41567-023-02048-w.
[49] Huderek D, Szczęsny S, Rato R. Spiking Neural Network Based on Cusp Catastrophe Theory. Found Comput Decis Sci 2019;44:273–84. https://doi.org/10.2478/fcds-2019-0014.
[50] Seregin D, Zorin V. Forecasting the resource of mechanical system by the Theory of Catastrophes. IOP Conf Ser Mater Sci Eng 2020;918:012075. https://doi.org/10.1088/1757-899X/918/1/012075.
[51] Zhu J, Lai C, Sun Y. Fault Mechanism Analysis for Manufacturing System Based on Catastrophe Model. Math Probl Eng 2019;2019:e2313581. https://doi.org/10.1155/2019/2313581.
[52] Cui H, Wan X, Xiong L. Modeling of the catastrophe of chip flow angle in the turning with double-edged tool with arbitrary rake angle based on catastrophe theory. Int J Adv Manuf Technol 2019;104:2705–14. https://doi.org/10.1007/s00170-019-04114-1.
[53] Xu J, Zhou Q, Tao J, Sun X, Zhao Q, Fu S, et al. Research on crack propagation law of rotating bending fatigue cropping process based on cusp catastrophe theory. Theor Appl Fract Mech 2022;118:103235. https://doi.org/10.1016/j.tafmec.2021.103235.
[54] Liang X, Wu JH, Zhong HB. Quantitative analysis of non-equilibrium phase transition process by the catastrophe theory. Phys FLUIDS 2017;29:085108.
[55] Liang X, Wu JH, Zhou G. Quantitative analysis for acoustic characteristics of porous metal materials by improved Kolmogorov's turbulence theory. Appl Acoust 2018;130:210–5.
[56] Zhou Z, Wu JH, Liang X, Lin M, Wang YL. Multi-dimensional complex phase transition model by catastrophe theory developing Kolmogorov turbulence theory. Mod Phys Lett B 2020:2050159.
[57] Pelat A, Gautier F, Conlon SC, Semperlotti F. The acoustic black hole: a review of theory and applications. J Sound Vib 2020;476:115316. https://doi.org/10.1016/j.jsv.2020.115316.
[58] Hao G. Research on structural vibration damping characteristics based on one-dimensional acoustic black hole effect. Nanjing University of Aeronautics and Astronautics; 2018.